Assembly of a functional Machupo virus polymerase complex

Philip J. Kranzusch[a], Andreas D. Schenk[b], Amal A. Rahmeh[a], Sheli R. Radoshitzky[c], Sina Bavari[c], Thomas Walz[b,d], and Sean P. J. Whelan[a,1]

[a]Departments of Microbiology and Molecular Genetics and [b]Cell Biology, and [d]The Howard Hughes Medical Institute, Harvard Medical School, Boston, MA 02115 and [c]US Army Medical Research Institute of Infectious Diseases, Fort Detrick, Frederick, MD 21702

Edited by Robert A. Lamb, Northwestern University, Evanston, IL, and approved October 6, 2010 (received for review May 21, 2010)

Segmented negative-sense viruses of the family *Arenaviridae* encode a large polymerase (L) protein that contains all of the enzymatic activities required for RNA synthesis. These activities include an RNA-dependent RNA polymerase (RdRP) and an RNA endonuclease that cleaves capped primers from cellular mRNAs to prime transcription. Using purified catalytically active Machupo virus L, we provide a view of the overall architecture of this multifunctional polymerase and reconstitute complex formation with an RNA template in vitro. The L protein contains a central ring domain that is similar in appearance to the RdRP of dsRNA viruses and multiple accessory appendages that may be responsible for 5′ cap formation. RNA template recognition by L requires a sequence-specific motif located at positions 2–5 in the 3′ terminus of the viral genome. Moreover, L-RNA complex formation depends on single-stranded RNA, indicating that inter-termini dsRNA interactions must be partially broken for complex assembly to occur. Our results provide a model for arenavirus polymerase–template interactions and reveal the structural organization of a negative-strand RNA virus L protein.

segmented negative-strand RNA virus | L protein structure | RNA binding | electron microscopy

The enzymatic machinery for RNA synthesis in viruses of the *Arenaviridae* and *Bunyaviridae*, two families of segmented negative-strand RNA viruses, is contained within a single large polymerase (L) protein. This protein is 250–450 kDa in size and is functionally analogous to the large polymerase proteins of nonsegmented negative-strand RNA viruses. The template for RNA synthesis consists of genomic RNA encapsidated by the viral nucleocapsid protein (NP). Structures of NP–RNA complexes from nonsegmented negative-sense RNA viruses indicate that L must transiently displace NP during RNA synthesis (1–5).

Arenavirus RNA synthesis initiates after the cytosolic delivery of two encapsidated segments, each associated with L. Each segment encodes two genes in an ambisense orientation divided by a highly structured intergenic region (IGR). Transcription initiates from the 3′ end of both the genomic and antigenomic templates and terminates at the IGR, yielding capped nonpolyadenylated transcripts (6). Heterogenic 5′ terminal mRNA sequences and dependency on host cell transcription reveal that L primes mRNA synthesis with cleaved host-cell RNA cap structures (7–9). Cytoplasmic extracts from infected cells support RNA synthesis and indicate L initiates replication at an internal element in the 3′ terminus to generate a pppGpC primer. This L-RNA complex then realigns with the terminal nucleotide to allow production of a full-length antigenomic RNA (10).

The terminal sequences of arenavirus and bunyavirus segments exhibit inverted complementarity and electron micrographs reveal that the termini interact (11–15). The resulting panhandle structure is thought to recruit L to the template for RNA synthesis. Consistent with this idea, substitutions at positions 13–19 of the 3′ end of a Lassa virus (LASV) genomic analog that diminish gene expression are complemented by changes at the 5′ terminus that restore the base pairing potential of the termini (16). A lack of in vitro biochemical assays has restricted direct tests of this model, and our understanding of arenavirus L protein and the polymerase–template complex remain limited.

Here, we report the overall architecture of an arenavirus L protein and define the RNA sequence requirements for template binding. We purified catalytically active Machupo virus (MACV) L and used negative stain electron microscopy (EM) to determine its organization. MACV L forms a core ring-structure that is decorated by an arm-like domain and small globular appendages. We propose that the central ring contains the RNA-dependent RNA polymerase (RdRP) and that the appendages are involved in cap formation. Using purified L, we reconstitute RNA synthesis and template complex formation in vitro and also establish a cell-based MACV replicon system. Using those assays, we define the RNA requirements for complex assembly and identify the promoter ssRNA motif 3′ N_{1-2}HKUG 5′ as essential for L recruitment. This work provides insight into RNA synthesis initiation that likely applies to all arenaviruses and bunyaviruses and reveals initial structural information regarding the L proteins of segmented negative-strand RNA viruses.

Results

Purification and EM Characterization of a Functional MACV L Protein. A cDNA of the MACV *L* gene was assembled in a T7 expression vector (pL) and used to support the replication of a modified MACV S segment encoding eGFP as described in *SI Methods* (Fig. 1*A*). The *L* gene encodes a functional polymerase as shown by the expression of eGFP in cells (Fig. 1*B*). A conserved motif present in the core polymerase domain has been predicted to coordinate a catalytically essential magnesium ion (17), and substitutions to this motif (SDD1328AAA) abolish eGFP production (Fig. 1*B*).

To characterize L structurally and biochemically, we purified the full-length protein from insect cells infected with a baculovirus vector (Fig. 1*C*). Establishment of an in vitro RNA synthesis assay, demonstrated that purified L possesses catalytic activity (Fig. 1*D*). This activity is greatly stimulated in the presence of GpC dinucleotide primer, as reported for RNA synthesis using cell extracts (10). Identical to the cell-based assay, the SDD mutation abolished RNA synthesis in vitro (Fig. 1*D*).

Highly purified, functional MACV L offered the opportunity to probe the structure of a segmented negative-sense L protein. EM images of L in negative stain showed monodispersed particles, permitting us to calculate averages that revealed a core ring-like domain decorated by appendages (Fig. 1*E* and Fig. S1).

Author contributions: P.J.K., A.A.R., T.W., and S.P.J.W. designed research; P.J.K. and A.D.S. performed research; S.R.R., and S.B. contributed new reagents/analytic tools; P.J.K., T.W., and S.P.J.W. analyzed data; and P.J.K. and S.P.J.W. wrote the paper.

The authors declare no conflict of interest.

This article is a PNAS Direct Submission.

[1]To whom correspondence should be addressed. E-mail: sean_whelan@hms.harvard.edu.

This article contains supporting information online at www.pnas.org/lookup/suppl/doi:10.1073/pnas.1007152107/-/DCSupplemental.

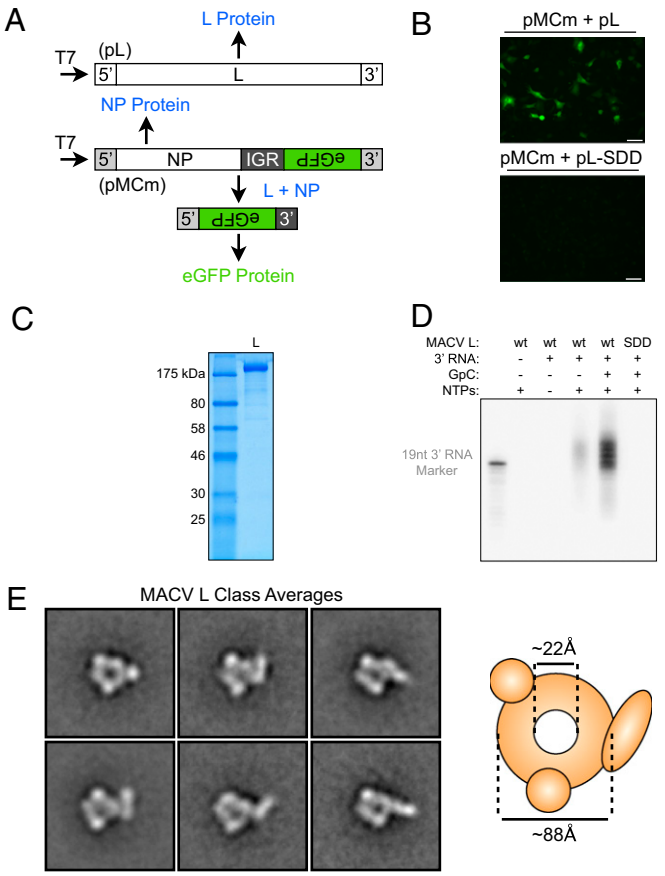

Fig. 1. Purification and EM characterization of a functional MACV L protein. (*A*) Schematic of replicon-based MACV RNA synthesis as described in text. (*B*) Epifluorescence miscroscopy images of cells expressing pMCm replicon in the presence of L (pL) or a catalytically inactivated mutant (pL-SDD). (Scale bars: 50 μm.) (*C*) Baculovirus-expressed purified MACV L (2 μg) analyzed by SDS/PAGE with Coomassie blue staining. (*D*) MACV in vitro RNA synthesis. Purified L (wt) or a catalytically inactivated mutant (SDD) was incubated with the corresponding reaction components in the presence of [α-^{32}P]GTP. Resulting RNA products were separated by denaturing gel electrophoresis. (*E*) Class averages of purified L in negative stain, each containing ≈100 particles. The side length of the individual images is 36 nm and the schematic displays approximate dimensions.

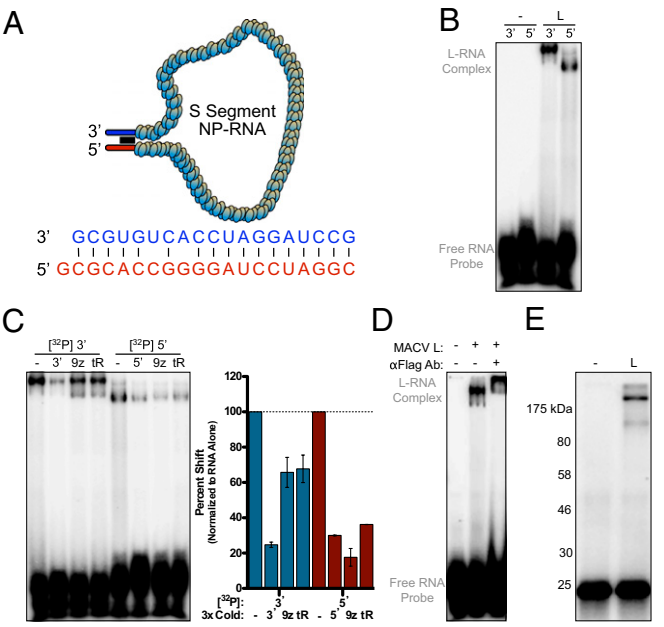

Fig. 2. Formation of a polymerase–template complex in vitro. (*A*) Cartoon of encapsidated S segment with dsRNA panhandle structure. (*B*) A gel shift assay of complex formation between L and RNA. Radiolabeled 3′ or 5′ RNA was incubated with buffer alone (-) or purified L (L), and resulting complexes were separated by nondenaturing gel electrophoresis. (*C*) Complex formation was competed with a 1:3 molar ratio of unlabeled RNA, pGEM9z transcript (9z), or yeast tRNA (tR). RNA binding was quantified with a PhosphorImager and graphed as values normalized to binding of the RNA probe alone. Error bars represent the SD from the mean of independent experiments. (*D*) L–3′ RNA complex formed in the presence of yeast tRNA was supershifted with an anti-FLAG antibody. (*E*) UV cross-linked L–3′ RNA complexes were denatured and analyzed by SDS/PAGE.

As other RdRPs have been shown to have ring-like structures (18), the core ring likely contains the RdRP activity, and flexibility results in multiple orientations of the arm-like domain (Fig. 1*E*). Since earlier work suggested that the polymerase may be involved in inter-termini interactions of arenaviral RNA segments (Fig. 2*A*) (12, 15), we next investigated potential sequence-specific interactions between purified polymerase and the RNA termini.

Formation of a Polymerase–Template Complex in Vitro. Using short RNA probes that correspond to the 3′ and 5′ genomic termini (Fig. 2*A*), we established an electrophoretic mobility shift assay for L template recognition. In the absence of competing RNA, L formed a complex with both probes (Fig. 2*B*). The L–3′ complex migrates slower than L-5′ complex, possibly due to differences in RNA sequence or alternatively distinct interactions with L (discussed in more detail below). Excess unlabeled 3′ RNA competed formation of the L–3′ complex, but a control RNA transcript (9z) or tRNA did not (Fig. 2*C*). Conversely, 9z and tRNA inhibited interaction with the 5′ terminus (Fig. 2*C*). The affinity of L for each terminus was determined by measuring equilibrium saturation binding, and L exhibited a stronger affinity for the 3′ RNA (149.9 ± 13.12 nM) than the 5′ terminus (229.1 ± 32.18 nM) (Fig. S2). Complex formation requires L (Fig. 2*B*), and its presence is verified by a shift in mobility upon addition of an antibody against the FLAG tag appended to the C terminus of L (Fig. 2*D*). The RNA was cross-linked to L upon exposure to ultraviolet radiation, further confirming that the complex contains L and RNA (Fig. 2*E*). These experiments demonstrate that L readily forms a sequence-specific complex with the 3′ terminus, whereas only a lower affinity interaction occurs with the 5′ end.

Template Requirements for Polymerase Binding. To probe the sequence requirements for L–3′ RNA interaction, we generated templates containing single-nucleotide substitutions at positions 1–7 (Fig. 3*A*). We chose these positions, because both a 10-nt 3′ RNA containing the correct sequence at positions 1–7 and a 19-nt 3′ RNA containing mutations at positions 8–19 bound with similar affinity as the 3′ 19-nt RNA (Fig. 3*B* and Fig. S3*A*). A single G3C mutation within this region abolished RNA synthesis in a LASV replicon system (16), and this mutation also inhibited recognition of the 19-nt MACV promoter sequence in vitro (Fig. 3*B*). Using a panel of 21 19-nt templates in which the sequence at position 1–7 was individually substituted for each possible nucleotide, we found that positions 2–5 contained important determinants of L binding (Fig. 3 *B* and *C*). Consistent with their critical nature for L–RNA recognition, mutations at these positions also disrupted RNA synthesis in the cell-based replicon assay, confirming the importance of L–RNA interactions reconstituted with purified components (Fig. S4). These experiments define a primary element at positions 2–5 of the 3′ promoter,

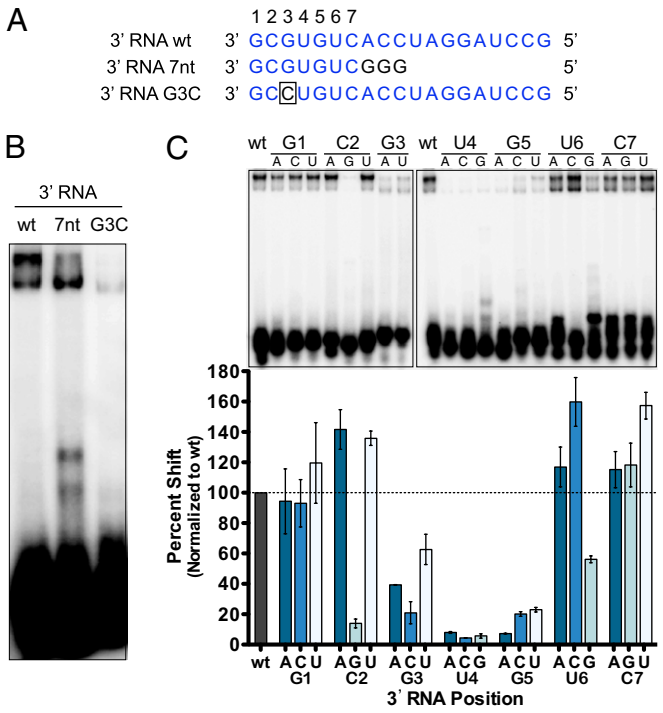

Fig. 3. Template requirements for polymerase binding. (*A*) RNA probes used to analyze template discrimination. (*B*) Labeled 3′ RNA probes were incubated with L in the presence of yeast tRNA, and complexes were separated and visualized as in Fig. 2*B*. (*C*) Resulting L–RNA complexes formed with a saturated mutagenesis panel of the first seven positions of the 19-nt 3′ RNA probe. RNA binding was quantified and graphed as in Fig. 2*C* and normalized as indicated.

3′ HKUG 5′ (where H and K represent "not G" and "G or U," respectively), which is required for efficient L binding.

Although the 5′ RNA formed a lower affinity interaction with L that was susceptible to competition, we were interested in determining whether L–5′ RNA interactions are also sequence-specific. We observed decreased binding between L and 5′ RNA with severe mutations or truncations at either terminus (Fig. S3*A*). These results indicate potential sequence-specific features important for L–5′ complex formation, yet individual adenosine mutations at each position failed to identify a specific motif (Fig. S3*B*). Thus, 5′ RNA binding occurs through low-affinity interactions that are resistant to single-nucleotide mutations but not excess nonspecific RNA, and is distinct from L–3′ RNA complex formation.

Polymerase Template Recognition Requires the Correct Positioning of the Sequence Element in Relation to the 3′ End. We hypothesized that the inhibitory nature of the C2G mutation may reflect the presence of three G's at the 3′ end of the template or the involvement of C2 in a base-pairing interaction with G5. Combining the C2G substitution with G1U or G5C failed to rescue the binding defect associated with C2G, indicating the guanylate is directly inhibitory (Fig. S5). The recognition element for L was sensitive to displacement from the 3′ terminus. Insertion of two or three adenylates at the 3′ terminus reduced template binding, whereas insertions at positions 6–8 had no such effect (Fig. S5). These data suggest that L binds to a linear sequence at the 3′ genomic RNA terminus.

Complex Formation with L Requires RNA Single-Stranded Nature. The prevailing model for RNA synthesis involves the formation of a termini dsRNA panhandle structure (Fig. 2*A*). Annealing the 3′ probe to excess 20-nt 5′ RNA, or 19-nt 5′ RNA lacking the nontemplated guanylate (5′Δ), inhibited L binding (Fig. 4*A*). To verify inhibition of 3′ RNA complex formation occurred through dsRNA formation and not by direct binding site competition with excess 5′ RNA, we used an additional 3′ probe that retains the high-affinity binding motif but harbors mutations at positions 8–19 (3′M). Competition experiments demonstrated that 3′M no longer forms dsRNA and is now resistant to 5′ RNA inhibition (Fig. 4*B*). Additionally, complex formation between L and labeled 5′ RNA is more resistant to 3′M competition than the pGEM9z transcript or tRNA (Figs. 2*C* and 4*B*). As L has a higher affinity for the 3′M probe than 5′ RNA (Fig. S3*A*), these

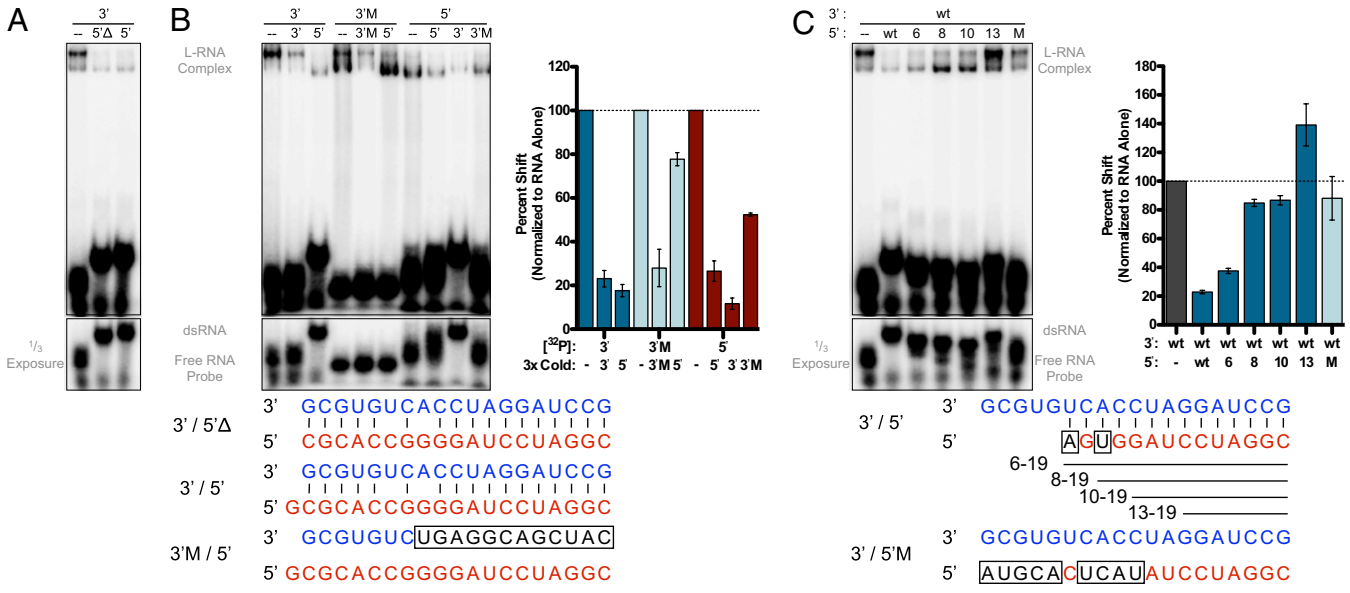

Fig. 4. Complex formation with L requires RNA single-stranded nature. (*A*) 3′ RNA probes were labeled and annealed to the corresponding 5′ RNA before incubation with L. Complexes were separated and visualized as in Fig. 2*B*. (*B* and *C*) Reactions were carried out as in *A* except RNA probes were incubated with a 1:3 molar ratio of labeled to unlabeled RNA as indicated. RNA binding was quantified and graphed as in Fig. 2*C* and normalized to RNA alone.

results indicate that the 3′ and 5′ RNAs are likely interacting at separate RNA-binding sites. The presence of both 3′ and 5′ RNA results in altered mobility of the L–RNA complex (Fig. 4), indicating that variations in complex mobility may represent alternative L–RNA bound states.

Inhibition of 3′ RNA recognition was also observed when dsRNA was formed with a truncated 5′ RNA (5′ 6) corresponding to nucleotides 6–19 of the genomic 5′ end (Fig. 4*C*). By contrast, duplexes formed with further truncated (5′ 8, 10, or 13) or mutated (5′M) RNA did not diminish L binding (Fig. 4*C*). These data show that the single-stranded nature of the genomic 3′ terminus is an important determinant of L protein binding and suggest that a complete panhandle structure would inhibit polymerase recruitment.

Discussion

We present the purification of a segmented negative-sense viral L protein and demonstrate the ability to recapitulate both catalytic and RNA-binding activities in vitro. Additionally, the EM images of MACV L presented here provide a view of the overall architecture of a segmented negative-strand RNA viral L protein and are a useful framework on which to assemble the structure of this class of viral polymerases. By reconstituting MACV polymerase–template complex assembly in vitro, we demonstrate that ssRNA character and a conserved 3′ $N_{1–2}$HKUG motif are critical for 3′ promoter recognition by L. We integrate our structural and biochemical findings together with those obtained by using cell-based RNA synthesis assays to provide information regarding the assembly of the arenavirus polymerase–template complex and initiation of RNA synthesis. Our findings are directly relevant to the understanding of L–template complex assembly for arenaviruses and bunyaviruses and will likely share parallels with viruses in the order *Mononegavirales*.

Biochemical and Structural Characterization of the L Protein. The purification of functional MACV L provides the opportunity to study arenavirus RNA synthesis reconstituted from purified components. RNA synthesis can be achieved with only L, a 19-nt 3′ RNA template, and NTPs, but is enhanced by GpC primer (Fig. 1*D*). This activity is abolished by mutations to a conserved SDD triad and supports the prediction that these residues are catalytically important for magnesium-ion coordination (17).

In addition to conserved catalytic motifs, homology with other template-dependent RNA polymerases has permitted structural modeling of the core L RdRP domain (17, 19). However, no structural data exists for any L protein. The EM averages of MACV L reveal a core ring domain decorated with two small globular appendages and a larger arm-like domain (Fig. 1*E* and Fig. S1). The core ring is ≈79 by 88 Å with a central channel 21–25 Å in diameter (Fig. 1*E*). As this ring is similar to the ring-like RdRP of reovirus and rotavirus (≈76 by 82 Å), it is likely to represent the MACV RdRP (18, 20, 21). These dimensions would then suggest that the genomic RNA must be released from NP before entry into the central channel.

We speculate that the domains decorating the core ring structure (Fig. 1*E* and Fig. S1) reflect accessory functions of L such as recognition and cleavage of host mRNA cap structures (8). The variation in appearance is consistent with the notion that flexible linkages within L connect the cap snatching activity and the RdRP. Such flexibility may permit the arm-like domain (Fig. 1*E*, *Lower*) to fold back onto the ring domain, resulting in a more globular appearance (Fig. 1*E*, *Upper*). We predict that the core RdRP domain will be maintained among all negative-strand RNA virus L proteins, whereas the accessory domains will vary, particularly between L proteins that catalyze cap synthesis (order *Mononegavirales*) (22, 23) and those that scavenge host mRNA cap structures (families *Arenaviridae* and *Bunyaviridae*) (7, 8, 24). Further support for these conclusions arises from parallel experiments with the L protein from a nonsegmented negative-sense RNA virus, vesicular stomatitis virus, where deletion fragments have mapped the RdRP to a similar ring domain and the capping apparatus to a different set of appendages (25). Although we cannot yet formally assign a function to any domain within the MACV L class averages, this initial glimpse at the overall architecture of L provides the groundwork to begin more detailed structural analysis.

RNA Template Discrimination. We provide direct biochemical demonstration that L forms a complex with the genomic RNA termini (Fig. 2). L forms a high-affinity, sequence-specific complex with 3′ RNA but interacts with the 5′ terminus with lower affinity (Fig. 2 and Figs. S2 and S3). The lower affinity binding of the 5′ terminus by L contrasts with the polymerase of influenza A virus (26, 27). For influenza A virus, interactions between the PB1 subunit of the polymerase and the 5′ terminus activate an mRNA cap-binding domain, indicating an alternative mechanism may exist for L (28, 29). Interactions with the 5′ terminus also regulate polyadenylation by the influenza A virus polymerase (30). Since arenaviral mRNAs are not polyadenylated and instead terminate at an internal hairpin, specific recognition of the 5′ end may not be required (6). As the placement of NP protein is unknown and these assays are not in the context of a full-length genomic segment, it is possible that other factors influence interactions with the 5′ terminus. However, once potential dsRNA interactions are abolished, the 3′ and 5′ RNA probes do not compete one another (Fig. 4 and Fig. S2); indicating that, as with influenza A virus polymerase-termini interactions, distinct RNA-binding sites may exist (27). Additionally, while affinity of L for the 3′ RNA is contained within a short linear sequence motif, binding of the 5′ RNA appears to be dependent on complex low affinity interactions that may explain why they are more easily competed by nonspecific RNA (Fig. 2*C* and Fig. S3).

L–3′ RNA binding requires a sequence and locality-dependent motif (3′ $N_{1–2}$HKUG 5′) (Fig. 3 and Fig. S5). Mutations to this sequence disrupt cell-based RNA synthesis in both MACV (Fig. S4) and LASV (16). The MACV termini have not been directly sequenced, but this motif is conserved in all experimentally determined arenavirus termini, including the closely related Junín virus (31). Mutations outside of this motif are tolerated for template recognition in vitro (Fig. 3 and Fig. S3), but single substitutions within the conserved 3′ 19-nt promoter still inhibit replicon-based RNA synthesis (Fig. S4) (16). A 3′ RNA U6G mutation, which naturally occurs in the S segment antigenomic promoter, resulted in slight inhibition of L binding (Fig. 3*C*). This variation may help account for altered promoter strength between genomic and antigenomic templates, but further experiments are required to fully address the effect of this position on viral transcription. Although it is possible that the exact requirements for promoter recognition extend beyond the conserved 3′ $C_2G_3U_4G_5$ binding site identified here, other conserved regions are likely more important for events downstream of template recognition.

Sequence-specific recognition of an internal 3′ motif is shared by other RNA viruses including rotavirus and the phage Φ6 (21, 32).

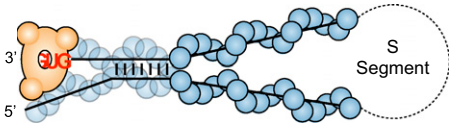

Fig. 5. Model of polymerase–template complex. Cartoon diagram of assembled arenavirus polymerase–template complex, as described in text. Recruitment of L occurs through an internal ssRNA $N_{1–2}$HKUG motif within the 3′ promoter that also serves as the site of internal initiation.

Rotavirus VP1 recognizes a nearly identical 3′ GUG motif, suggesting that interactions in the entry channel of VP1 may parallel the template-binding site of MACV L. After RNA binding, rotavirus VP1 is thought to undergo a VP2-mediated structural rearrangement that repositions the template for initiation (21). In an analogous repositioning, L may prime at the $G_3U_4G_5$ motif before realigning the template to initiate synthesis at the extreme 3′ terminus. This suggestion is consistent with the prime-and-realign model of RNA synthesis in which L initiates on the cytosine at position 2 to create a pppGpC primer that is realigned so that the underlined C is opposite the 3′ terminal G (10). Our data also support this model of initiation because RNA synthesis with purified MACV L is greatly stimulated by the addition of GpC primer (Fig. 1*D*). As insertions greater than a single nucleotide at the 3′ terminus (Fig. S5 *E* and *F*) were not tolerated by L, limits to template recognition could play a role in dictating the L active site position and internal priming event. Following initiation, structural organization of the RNA binding cavity would then guide realignment of the initiation complex.

Promoter Complex Assembly. For arenaviruses and bunyaviruses, the potential dsRNA structure formed between genomic termini (Fig. 2*A*) is thought to be required for recruitment of L (33, 34). Our findings are incompatible with the direct interaction of L with this structure, as duplexed RNA inhibits L binding to the 3′ terminus (Fig. 4). Single-stranded RNA character is essential for L–RNA complex formation in vitro, yet potential base pairing interactions between positions 13–19 of the termini are important for efficient LASV replicon-based RNA synthesis (16). Our work demonstrates that dsRNA character in this region does not impact L recruitment (Fig. 4), suggesting that the termini would only need to be partially unwound to accommodate L binding (Fig. 5). Relative dsRNA character within the promoter may regulate polymerase transcriptional activity and shield the L binding site. Consistent with this idea, mutations to positions 6 and 8 of the LASV 3′ terminus that restore interactions with the 5′ terminus inhibit gene expression (16). Instead of polymerase recruitment, we suggest that the panhandle structure may facilitate ongoing RNA synthesis. The events after initiation are unknown, but a dsRNA panhandle structure may serve to maintain the termini in close proximity so that as L completes RNA synthesis it is able to reengage the high-affinity 3′ terminus binding site. Through this process, the combination of a lower affinity of L for the 5′ terminus and dsRNA interactions between termini may facilitate polymerase reloading (Fig. S6). The ability to recapitulate arenaviral RNA synthesis from purified components offers the opportunity to begin testing these models.

Applications of the Reconstruction of MACV RNA Synthesis. Our electron microscopy characterization provides an architectural map of an arenavirus L that reveals a structural organization potentially shared by all negative-strand RNA viral L proteins. Combined with in vitro RNA synthesis, assembly of the polymerase–template complex and a complementary cell-based replicon assay, this work represents a significant technical advancement in our ability to dissect mechanistic details of arenaviral RNA synthesis. Additionally, MACV and other New World hemorrhagic fever arenaviruses cause severe disease and represent an important class of emerging human pathogens (35). The tools developed here are readily adaptable for high-throughput screening and represent an important step along the path to rescue of recombinant MACV from cDNA. The 19-nt promoter element is conserved among all viruses of the *Arenaviridae* family, suggesting that recognition of the 3′ motif occurs through shared properties of the cognate L proteins. This highly conserved protein–RNA interface may thus represent an attractive therapeutic target.

Methods

Protein Purification and Single-Particle Electron Microscopy. MACV L was expressed with a recombinant baculovirus and purified from *Sf*21 cells as described in *SI Methods*. Purified L samples were adsorbed for 10 s to glow-discharged, carbon-coated copper EM grids and stained with 0.75% (wt/vol) uranyl formate as described (36). Images were collected on a Tecnai T12 electron microscope and recorded on imaging plates at 67,000× according to *SI Methods*. A total of 8,871 particles were interactively selected by using BOXER (37). Individual particles were windowed into 80 × 80 pixel images by using SPIDER (38), rotationally and translationally aligned, and subjected to 10 cycles of multireference alignment. Each round of multireference alignment was followed by K-means classification into 100 classes.

L-RNA Gel Shift Assay. The 7-nt 3′ RNA and pGEM9z probes were prepared as described in *SI Methods*; all other 3′ and 5′ RNA probes were chemically synthesized (IDT). RNAs were labeled with T4 PNK (NEB) and [γ-^{32}P]ATP for 1.5 h at 37 °C before phenol-chloroform extraction and ethanol precipitation. Labeled RNA (6 pmol) was denatured at 65 °C for 3 min and cooled on ice. Binding buffer [50 mM Tris·HCl at pH 7, 40 mM NaCl, 5 mM Mg$(OAc)_2$, 10 mM KCl, 1 mM DTT, and 0.1 mg/mL BSA (NEB)] was added and included 10 μg of yeast tRNA (Sigma) only when indicated. In a final reaction volume of 10 μL, 0.15 μg of purified L was added and reactions were incubated at 25 °C for 30 min before separation on a 6% nondenaturing polyacrylamide gel. For supershift reactions, complexes were incubated with 2 μg of α-Flag M2 antibody (Sigma) for 10 min before separation. Alternatively, reactions were cross-linked in the presence of 10 μg of yeast tRNA for 15 min with a 254nm UV light positioned 5 cm away, and samples were denatured and separated by 10% SDS/PAGE. Dried gels were visualized with a PhosphorImager and quantified by using ImageQuant (Amersham). Where indicated, dsRNA duplexes were formed by heating 6 pmol labeled 3′ RNA with 18 pmol unlabeled 5′ RNA to 95 °C for 5 min in 10 mM Tris at pH 8 and 5 mM NaCl and cooled to 4 °C at 0.1 °C/s.

In Vitro RNA Synthesis. Unlabeled 19-nt 3′ RNA was denatured at 65 °C for 3 min and cooled on ice. Transcription buffer [50 mM Tris·HCl at pH 7, 40 mM NaCl, 5 mM $MnCl_2$, 10 mM KCl, 1 mM DTT, and 0.1 mg/mL BSA (NEB)] was added and, in a final reaction volume of 10 μL, 0.35 μg of purified L was added and reactions were incubated at 25 °C for 30 min. After initial incubation, 1.0 μL of [α-^{32}P]GTP (≈10 μCi) was added to each reaction, followed by the addition of cold NTPs (1 mM ATP/CTP/UTP) where indicated, and reactions were incubated at 30 °C for 2 h. Where indicated, reactions included 40 μM GpC dinucleotide primer (Dharmacon). Reactions were treated with 8 units of alkaline phosphatase (NEB) at 37 °C for 45 min and then 2.4 μg of proteinase K (Sigma) at 45 °C for 45 min followed by phenol-chloroform extraction and ethanol precipitation. RNA was washed 3 times with 70% ethanol and resuspended in 10 μL of dH_2O before separation by denaturing 20% polyacrylamide gel electrophoresis.

ACKNOWLEDGMENTS. This study was supported by National Institutes of Health Grants AI057159 and AI059371. S.P.J.W. is a recipient of a Burroughs Wellcome Investigators Award, A.D.S. is supported by a fellowship from the Swiss National Science Foundation, and T.W. is a Howard Hughes Medical Institute Investigator. We acknowledge the exceptional support by Robin Ross and Lauren Perry (New England Regional Center of Excellence for Biodefense and Emerging Infectious Diseases). A portion of the research described herein was sponsored by the Defense Threat Reduction Agency, JSTO-CBD (project number 4.10022_08_RD_B and TMTI0048_09_RD_T to S.B.).

1. Rudolph MG, et al. (2003) Crystal structure of the borna disease virus nucleoprotein. *Structure* 11:1219–1226.
2. Albertini AA, et al. (2006) Crystal structure of the rabies virus nucleoprotein-RNA complex. *Science* 313:360–363.
3. Green TJ, Zhang X, Wertz GW, Luo M (2006) Structure of the vesicular stomatitis virus nucleoprotein-RNA complex. *Science* 313:357–360.
4. Ye Q, Krug RM, Tao YJ (2006) The mechanism by which influenza A virus nucleoprotein forms oligomers and binds RNA. *Nature* 444:1078–1082.
5. Tawar RG, et al. (2009) Crystal structure of a nucleocapsid-like nucleoprotein-RNA complex of respiratory syncytial virus. *Science* 326:1279–1283.
6. Iapalucci S, López N, Franze-Fernández MT (1991) The 3′ end termini of the Tacaribe arenavirus subgenomic RNAs. *Virology* 182:269–278.

7. Raju R, et al. (1990) Nontemplated bases at the 5′ ends of Tacaribe virus mRNAs. *Virology* 174:53–59.
8. Lelke M, Brunotte L, Busch C, Günther S (2010) An N-terminal region of Lassa virus L protein plays a critical role in transcription but not replication of the virus genome. *J Virol* 84:1934–1944.
9. Mersich SE, Leon ME, Coto C (1979) Cell nucleus participation in the multiplication of the arenavirus tacaribe. *FEMS Microbiol Lett* 6:205–207.
10. Garcin D, Kolakofsky D (1992) Tacaribe arenavirus RNA synthesis in vitro is primer dependent and suggests an unusual model for the initiation of genome replication. *J Virol* 66:1370–1376.
11. Hewlett MJ, Pettersson RF, Baltimore D (1977) Circular forms of Uukuniemi virion RNA: An electron microscopic study. *J Virol* 21:1085–1093.
12. Young PR, Howard CR (1983) Fine structure analysis of Pichinde virus nucleocapsids. *J Gen Virol* 64:833–842.
13. Pettersson RF, von Bonsdorff CH (1975) Ribonucleoproteins of Uukuniemi virus are circular. *J Virol* 15:386–392.
14. Obijeski JF, Bishop DH, Palmer EL, Murphy FA (1976) Segmented genome and nucleocapsid of La Crosse virus. *J Virol* 20:664–675.
15. Palmer EL, Obijeski JF, Webb PA, Johnson KM (1977) The circular, segmented nucleocapsid of an arenavirus-Tacaribe virus. *J Gen Virol* 36:541–545.
16. Hass M, et al. (2006) Mutational analysis of the lassa virus promoter. *J Virol* 80: 12414–12419.
17. Müller R, Poch O, Delarue M, Bishop DH, Bouloy M (1994) Rift Valley fever virus L segment: Correction of the sequence and possible functional role of newly identified regions conserved in RNA-dependent polymerases. *J Gen Virol* 75:1345–1352.
18. Ferrer-Orta C, Arias A, Escarmís C, Verdaguer N (2006) A comparison of viral RNA-dependent RNA polymerases. *Curr Opin Struct Biol* 16:27–34.
19. Hass M, Lelke M, Busch C, Becker-Ziaja B, Günther S (2008) Mutational evidence for a structural model of the Lassa virus RNA polymerase domain and identification of two residues, Gly1394 and Asp1395, that are critical for transcription but not replication of the genome. *J Virol* 82:10207–10217.
20. Tao Y, Farsetta DL, Nibert ML, Harrison SC (2002) RNA synthesis in a cage—structural studies of reovirus polymerase lambda3. *Cell* 111:733–745.
21. Lu X, et al. (2008) Mechanism for coordinated RNA packaging and genome replication by rotavirus polymerase VP1. *Structure* 16:1678–1688.
22. Ogino T, Banerjee AK (2007) Unconventional mechanism of mRNA capping by the RNA-dependent RNA polymerase of vesicular stomatitis virus. *Mol Cell* 25:85–97.
23. Li J, Rahmeh A, Morelli M, Whelan SP (2008) A conserved motif in region v of the large polymerase proteins of nonsegmented negative-sense RNA viruses that is essential for mRNA capping. *J Virol* 82:775–784.
24. Duijsings D, Kormelink R, Goldbach R (2001) In vivo analysis of the TSWV cap-snatching mechanism: Single base complementarity and primer length requirements. *EMBO J* 20:2545–2552.
25. Rahmeh AA, et al. Molecular architecture of the vesicular stomatitis virus RNA polymerase. *Proc Natl Acad Sci USA* 107:20075–20080.
26. Tiley LS, Hagen M, Matthews JT, Krystal M (1994) Sequence-specific binding of the influenza virus RNA polymerase to sequences located at the 5′ ends of the viral RNAs. *J Virol* 68:5108–5116.
27. Li ML, Ramirez BC, Krug RM (1998) RNA-dependent activation of primer RNA production by influenza virus polymerase: Different regions of the same protein subunit constitute the two required RNA-binding sites. *EMBO J* 17:5844–5852.
28. Hagen M, Chung TD, Butcher JA, Krystal M (1994) Recombinant influenza virus polymerase: Requirement of both 5′ and 3′ viral ends for endonuclease activity. *J Virol* 68:1509–1515.
29. Cianci C, Tiley L, Krystal M (1995) Differential activation of the influenza virus polymerase via template RNA binding. *J Virol* 69:3995–3999.
30. Pritlove DC, Poon LL, Fodor E, Sharps J, Brownlee GG (1998) Polyadenylation of influenza virus mRNA transcribed in vitro from model virion RNA templates: Requirement for 5′ conserved sequences. *J Virol* 72:1280–1286.
31. Albariño CG, et al. (2009) Efficient reverse genetics generation of infectious junin viruses differing in glycoprotein processing. *J Virol* 83:5606–5614.
32. Butcher SJ, Grimes JM, Makeyev EV, Bamford DH, Stuart DI (2001) A mechanism for initiating RNA-dependent RNA polymerization. *Nature* 410:235–240.
33. Auperin D, et al. (1982) Analyses of the genomes of prototype pichinde arenavirus and a virulent derivative of Pichinde Munchique: Evidence for sequence conservation at the 3′ termini of their viral RNA species. *Virology* 116:363–367.
34. Lee KJ, Novella IS, Teng MN, Oldstone MB, de La Torre JC (2000) NP and L proteins of lymphocytic choriomeningitis virus (LCMV) are sufficient for efficient transcription and replication of LCMV genomic RNA analogs. *J Virol* 74:3470–3477.
35. Geisbert TW, Jahrling PB (2004) Exotic emerging viral diseases: Progress and challenges. *Nat Med* 10(12, Suppl):S110–S121.
36. Ohi M, Li Y, Cheng Y, Walz T (2004) Negative staining and image classification—powerful tools in modern electron microscopy. *Biol Proced Online* 6:23–34.
37. Ludtke SJ, Baldwin PR, Chiu W (1999) EMAN: Semiautomated software for high-resolution single-particle reconstructions. *J Struct Biol* 128:82–97.
38. Frank J, et al. (1996) SPIDER and WEB: Processing and visualization of images in 3D electron microscopy and related fields. *J Struct Biol* 116:190–199.